Electronic Supplementary Material (ESI) for Journal of Materials Chemistry B.

Electronic Supporting Information for

NIR-Light Active Hybrid Nanoparticles for Combined Imaging and Bimodal Therapy of Cancerous Cells

A. Topete,[a] *D. Melgar,*[a,§] *M. Alatorre-Meda,*[a,#] *P. Iglesias,*[b] *B. Argibay,*[c] *S. Vidawati,*[a] *S. Barbosa,*[a*] *J. A. Costoya,*[b] *P. Taboada,*[a*] *V. Mosquera*[a]

[a] Grupo de Física de Coloides y Polímeros, Departamento de Física de la Materia Condensada, Universidad de Santiago de Compostela, Santiago de Compostela, 15782, Spain.

[b] Grupo de Oncología Molecular, Centro de Investigación en Medicina Molecular y Enfermedades Crónicas (CIMUS), Universidad de Santiago de Compostela, Santiago de Compostela, 15782, Spain.

[c] Laboratorio de Investigación en Neurociencias Clínicas, Hospital Clínico Universitario de Santiago de Compostela, 15782, Spain.

A. Experimental section

Characterization of NPs: The concentration of PLGA NPs was determined from the solvent's and the sample's specific viscosities (Eq. 1) (measured in triplicate) and the hydrodynamic radius of the NPs using the Einstein's viscosity relationship for spheres (Eq. 2):[1]

$$\eta_{sp} = 1 - \frac{\eta}{\eta_0} \quad (1)$$

$$\eta_{sp} = 2.5\left(\frac{n_2}{V}\right)V_e \quad (2)$$

where η is the sample's dynamic viscosity, η_0 is the solvent viscosity, $\frac{n_2}{V}$ is the number of equivalent spheres per volume unit, $Ve = \frac{4}{3}\pi R_e^2$ is the volume of an equivalent sphere, and R_e is the hydrodynamic radius of an equivalent sphere. The UV-vis absorption of different dilutions of NPs was measured and plotted versus the calculated concentrations to prepare a calibration curve, thus, NP concentrations could be calculated from UV-vis measurements.

B. Effect of PLGA molecular weight and concentration

The effect of polymer molecular weight on the size and zeta potential of the resulting PLGA NPs was rather small, the NP diameters being largely determined by the primary size of the formed emulsion droplets (Table S1). On the other hand, an increase in PLGA concentration causes a significant increase in NPs diameters from 146 ± 4 nm at 10 mg/mL PLGA to 191 ± 5 nm at 100 mg/mL (Figure S1a).[2] Increasing the PLGA concentration enhances the viscous resistance of the emulsion

mixture thereby absorbing the agitation energy which, in turn, leads to the reduction in shear stress and to droplets with larger size and, hence, to larger NPs. Also, a significant decrease in NP zeta potential values was noted from -23.5 ±0.9 mV at 10 mg/mL to −34.5 ±1.7 mV at 100 mg/mL, respectively. This decrease is consistent with the presence of more charged carboxylic groups of PLGA chains in the NPs, which ensures their colloidal stabilization.

C. Effect of organic and aqueous phases volumes

The effect of both organic and aqueous phase volumes (at constant polymer and stabilizer concentrations of 10 and 25 mg/mL, respectively) on the characteristics of the resulting NPs is shown in Figure S1b-c. An increase in both aqueous and organic phase volumes involved a reduction in both NP size and zeta potential. For the organic phase volume, the reduction in both size and zeta potential occurs up to a critical value (40 mL) provided the optimal diffusion of the PLGA polymer chains under such conditions, which favors the formation of smaller nanodroplets. Above such threshold value, the NP size started to increase from 90 ± 3 to 123 ± 6 nm due to the formation of reverse emulsion droplets of larger sizes.

Table S1: Sizes, polydispersity indexes (PDI) and zeta potential values of PLGA NPs obtained with several PLGA polymers of different molecular weights and composition at a polymer concentration of 10 mg/ml.

PL-GA Proportion	Mw (kDa)	r_h (nm)	PDI	Zeta Potential (mV)
50-50	7-17	82 ± 3	0.060	-28.3 ± 2.3

50-50	24-38	75 ± 4	0.045	-29.9 ± 1.4
50-50	38-54	81 ± 3	0.038	-31.5 ± 0.9
50-50	40-75	83 ± 2	0.061	-33.8 ± 1.9
75-25	4-15	75 ± 4	0.027	-22.0 ± 0.6
75-25	66-107	77 ± 4	0.021	-18.4 ± 1.1

D. Effect of type and concentration of stabilizer concentration

The increase in F127 stabilizer concentration slightly changed the average NP sizes from ca. 150 ± 9 to 162 ± 11 nm between 2.5 and 25 mg/mL of added F127; at larger F127 concentrations NP sizes increased up to ca. 190 ± 15 nm (Figure S1d). This effect can be ascribed to the enhancement of the aqueous solution viscosity, which results in a reduction of the net shear stress and the corresponding increase in particle size.[3] However, other researchers have reported the opposite effect[2b,3,4] originated from the orientation of more stabilizer molecules in the interfacial area which decreases the interfacial tension and, hence, favours the formation of smaller droplets.[5] It seems clear that the observed effect must be a balanced of both opposite effects.

On the other hand, while increasing F127 concentration the zeta potential first slightly increases (from −33.8 ±1.8 mV at 2.5 mg/mL to −30.0 ±1.7 mV at 25 mg/mL) and, then, it steeply rises up to -23.5 ±1.2 mV at 50 mg/mL F127. This decrease in the net electric charge arises from the successive number of F127 layers on the PLGA NPs which progressively shield the carboxyl groups of PLGA chains

(bare PLGA NPs have a zeta potential of ca. -45.0 ± 2.8 mV).[6] The type of stabilizer also had some influence on the physico-chemical properties of the resulting NPs. Under standard preparation conditions, F127-stabilized PLGA NPs display lower sizes than PVA-stabilized ones (Table S2). Such size reduction could stem from the amphiphilicity of the Pluronic copolymer, whose hydrophobic blocks might penetrate the core-shell NP interface and interact with the PLGA chains given rise to more compact NPs. As a consequence, the hydrophilic blocks would shield the carboxylic groups of PLGA chains to a lesser extent, as observed from the smaller (more negative) zeta potential values found for F127-stabilized NPs. In addition, the purification process of the stabilizer excess also influenced the final size and charge of the resulting NPs (Table S2).

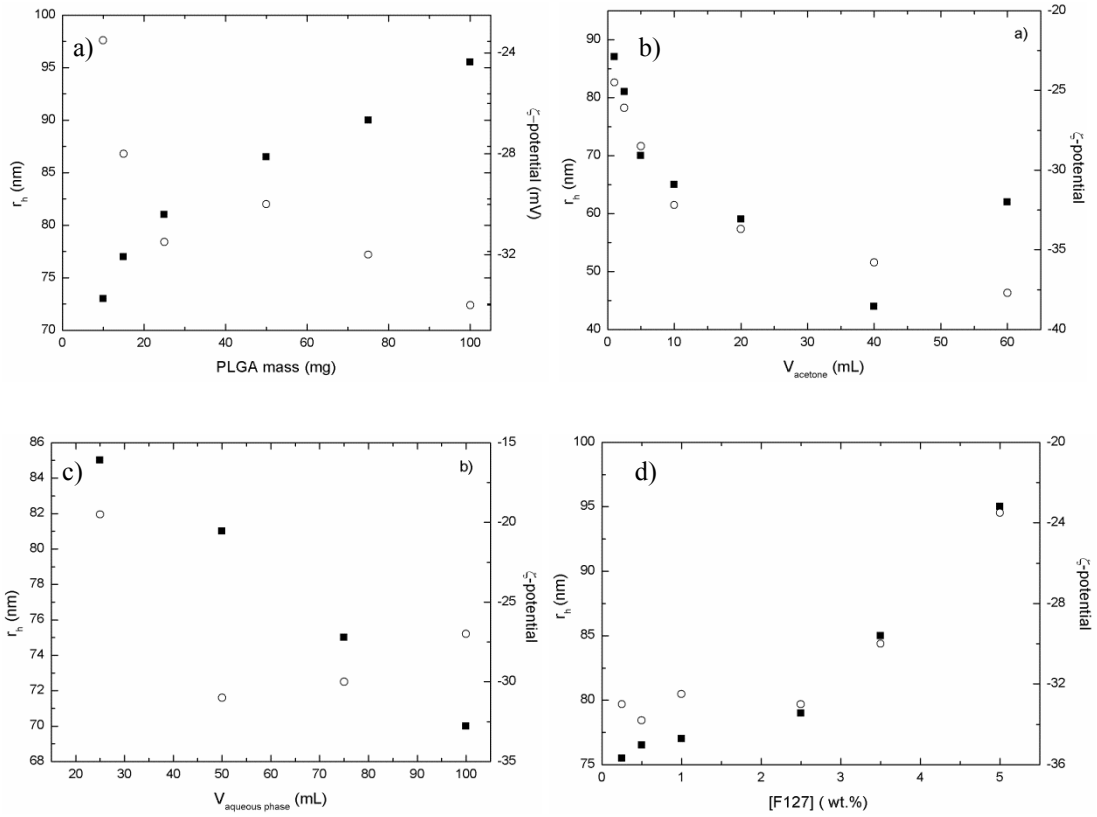

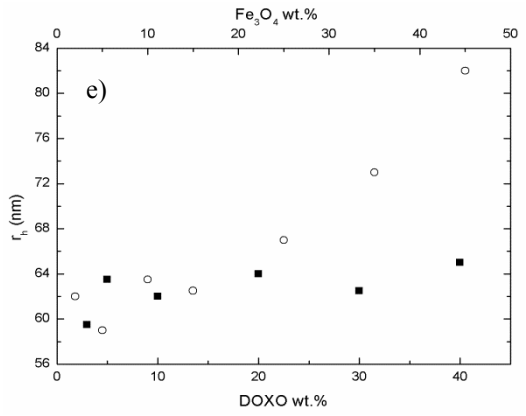

Figure S1: a) Effect of PLGA mass on the size (○) and zeta potential (ᔓ) of PLGA NPs. Effect of b) organic phase (acetone) and c) aqueous phase volumes on the size (○) and surface charge (ᔓ) of PLGA NPs. In b) $V_{aqueous\ phase}$ = 50 mL, and in c) $V_{acetone}$ = 2.5 mL. d) Effect of F127 stabilizer concentration on the size (○) and surface charge (ᔓ) of PLGA NPs ($V_{aqueous\ phase}$ = 50 mL, $V_{acetone}$ = 2.5 mL). e) Effect of DOXO (○) and SPIONs (ᔓ) loaded concentration on the size of the resulting DXSP-PLGA NPs.

Table S2: Effect of stabilizer type and purification process on the size and shape of DXSP-PLGA NPs at a stabilizer concentration of 10 mg/mL.

Stabilizer	**Centrifugation cycle**	**r_h (nm)**	**Zeta Potential (mV)**
F127	1	106 ± 6	-19.1 ± 1.2
F127	2	95 ± 5	-22.7 ± 1.5
PVA	1	114 ± 7	-8.8 ± 1.0
PVA	2	105 ± 6	-9.8 ± 0.7

E. Effect of initially loaded DOXO and SPIONs

The particle size and zeta potential of PLGA NPs loaded with SPIONs and the chemotherapeutic drug DOXO (DXSP-PLGA NPs) was found to be smaller than that of bare polymeric NPs (Figure S1e), and dependent on the molecular weight of the

PLGA polymer (Table S3). The size NP reduction upon cargo incorporation can stem from a compactation of the PLGA core through the enhancement of hydrophobic interactions between PLGA chains, drug molecules and oleic acid chains anchored on the SPIONs surfaces.[7] This enhanced hydrophobic interactions inside the polymeric matrix might involve a PLGA chain reconfiguration while exposing additional hydrophilic charged carboxylic groups to the aqueous medium, giving rise to lower (more negative) zeta potential values.[8]

Table S3: Sizes, polidispersities (PDI) and zeta potential values of DXSP-PLGA NPs obtained with several 50:50 PLGA polymers of different molecular weight and composition loaded with 10 wt.% DOXO and 2 wt.% Fe_3O_4 NPs at a polymer concentration of 10 mg/mL.

Mw (kDa)	**rh (nm)**	**PDI**	**Zeta Potential (mV)**
7-17	55.2 ± 0.7	0.030	-45.3 ± 3.2
24-38	60.7 ± 0.7	0.028	-47.6 ± 2.9
38-54	62.1 ± 1.0	0.030	-40.0 ± 2.1
40-75	77.0 ± 1.4	0.062	-33.9 ± 1.9

On the other hand, the capability of the nanocarriers to entrap sufficient active drug concentration to exert their therapeutic activity is crucial for their clinical application. In this regard, as both the initial DOXO and SPIONs concentrations increase the entrapped amount of the respective cargos first rised and, then, reached a quasi-plateau region (Figure S2). This behavior is favored by an enhanced cargo

miscibility inside the polymeric core promoting, at first, a larger incorporation in the organic phase.

However, the increase in loading capacity (LC) is not proportional to the increase of initial drug content during formulation, thus, the entrapment efficiencies (EE) decreased. The maximum entrapped DOXO and SPIONs concentrations were found to be approximately of ca. 18 wt.% and ca. 9.5 wt.%, respectively. We have also noted an important increase in both LC and EE when co-loading both DOXO and SPIONs inside the PLGA matrix. For example, a drug EE of 95% and a LC of 8.9% was reached in the presence of 1.5 wt.% of oleic acid-stabilized SPIONs (as measured by ICP-MS), compared with a 39% EE and 3.2% LC when the SPIONs were not loaded inside the PLGA NPs. Provided that the drug content in NPs is affected by drug-polymer interactions and DOXO miscibility inside the polymeric matrix,[9] it seems that the establishment of enhanced hydrophobic interactions between the different components inside the NPs would give rise to a synergistic effect which favours the enhanced solubilization ability of the present hybrid nanovehicle, as commented previously.

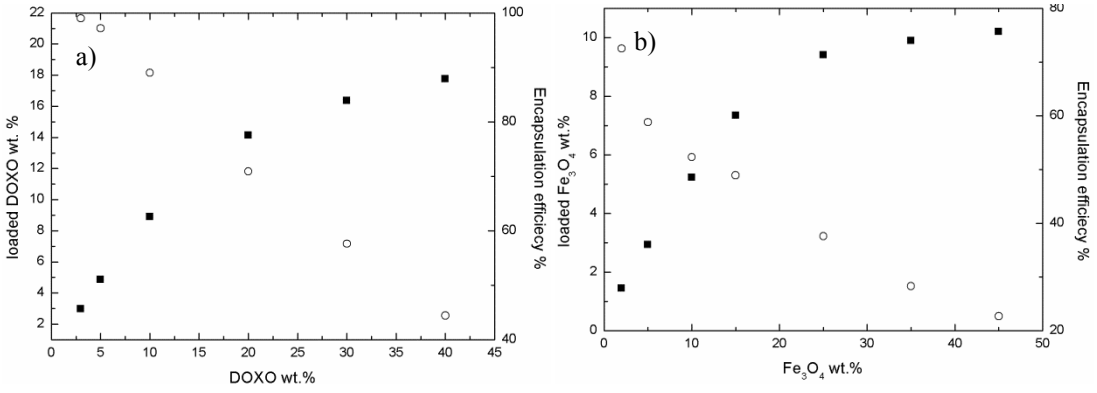

Figure S2: Loading capacity (O) and encapsulation efficiency (ᘓ) of PLGA NPs at different a) DOXO and b) SPIONs concentrations. In a), SPIONs concentration is kept constant at 5 wt.% whilst in b) DOXO concentration is fixed at 10 wt.%.

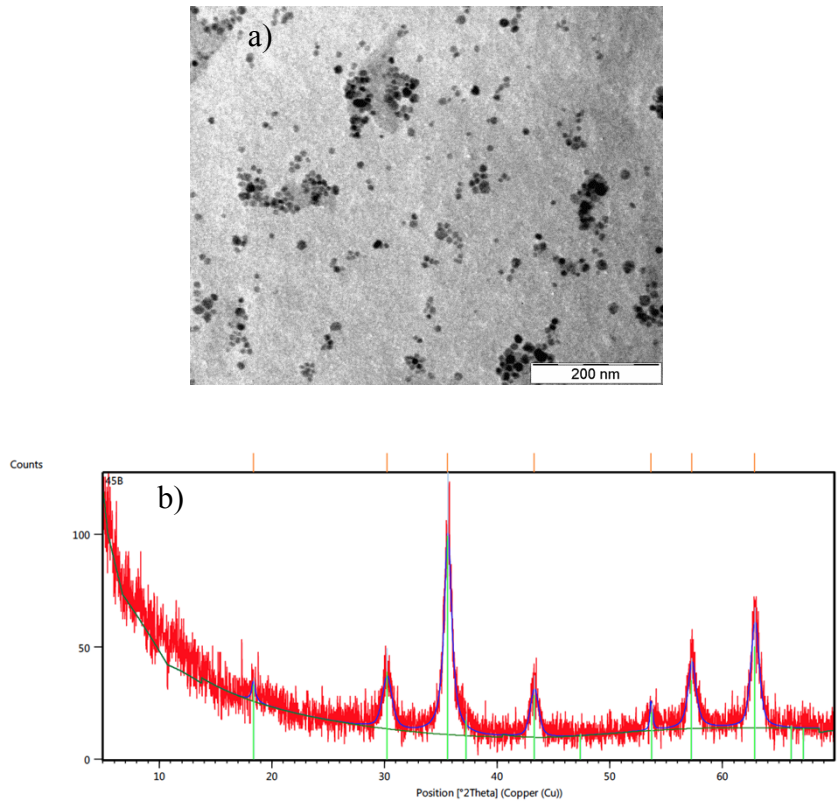

Figure S3: a) TEM image of oleic acid-stabilized Fe_3O_4 NPs; b) Powder X-ray diffractogram (XRD) of as-synthesised oleci acid stabilized Fe_3O_4 NPs. Green lines indicate the position of the characteristic peaks in the diffractogram whereas brown vertical lines denote the characteristic peaks of magnetite X-ray diffraction pattern.

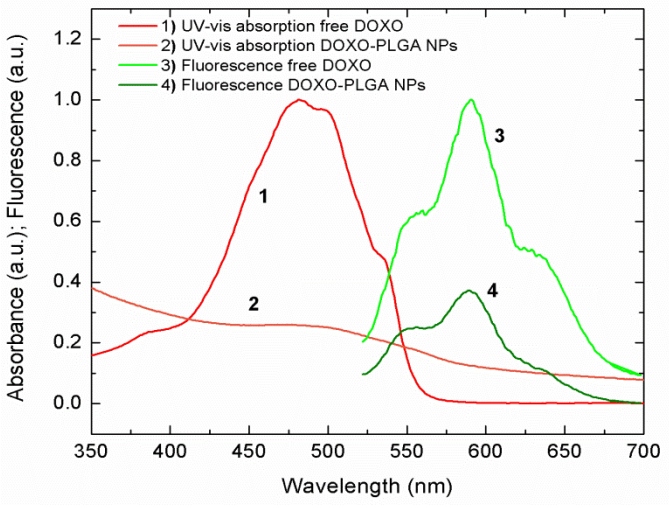

Figure S4: Fluorescence emission spectra of free DOXO, free ICG, and DXSP-PLGA-ICG NPs at excitation wavelengths 490 nm and 760 nm.

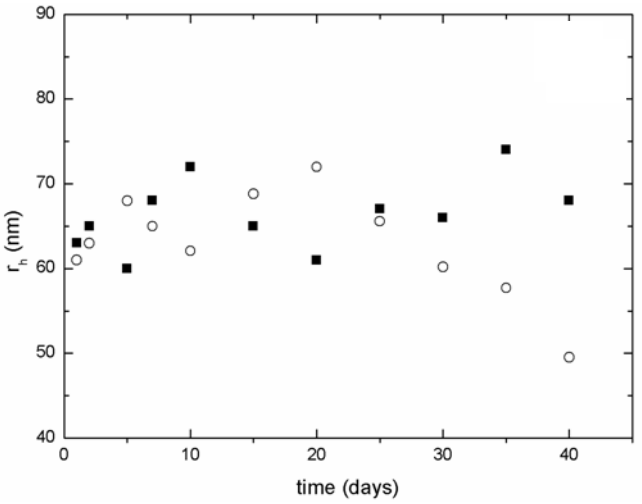

Figure S5: Size evolution of PLGA-based hybrid NPs in aqueous serum-containing (10% (v/v) FBS) medium of pH (O) 7.4 and (ᔓ) 5.5.

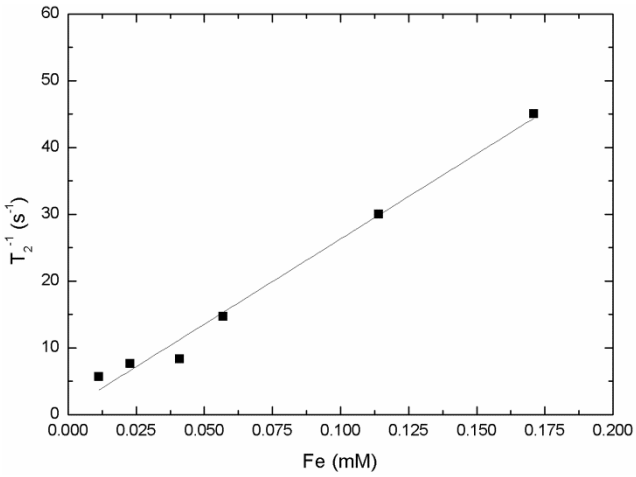

Figure S6: Spin-spin relaxivity (r_2) of the hybrid NPs.

F. Release kinetics

DOXO release kinetics could be fine-tuned by simply changing the molecular weight of the PLGA core. The burst phase and, consequently, the amount of DOXO released at short incubation times may largely be increased by decreasing the molecular weight of the PLGA chains used to form the polymeric core of the NPs

(Figure S7). This behavior is related to the combination of several effects such as the decrease in the viscosity and compactation of the polymeric core, and a weakening of the hydrophobic interactions between PLGA chains and DOXO molecules as the PLGA molecular weight decreases, which favors an enhanced mobility of drug molecules inside the PLGA core and a larger partition of DOXO molecules from the organic phase into the aqueous one. Hence, we decided to use PLGA NPs composed of a relatively large molecular weigth PLGA polymer (38-54 kDa) to reduce drug leakage during the burst phase. For this type of PLGA NPs, it has been shown that the cargo release typically occurs via a combination of diffusion and erosion through hydrolysis of the ester bonds in the polymer backbone. Also, the PLGA copolymer configuring the reservoir for DOXO drug molecules shows a glass-transition temperature (T_g) of ca. 45 ºC, which reduces the drug leakage during circulation and release when needed, that is, in the vicinity of tumors where acidic hydrolysis of the polymeric matrix can be enhanced.

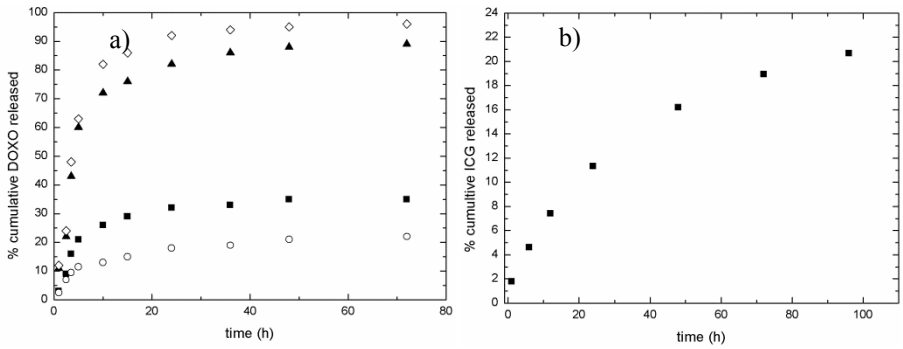

Figure S7: a) *In vitro* release kinetics of DOXO from DXSP-PLGA-ICG NPs of different copolymer molecular weight in aqueous serum-containing (10% (v/v) FBS) medium at pH 7.4. (ᔓ) 40-75; (O) 38-54; (□) 24-38 and (❋) 7-17 kDa. b) *In vitro* release kinetics of ICG from DXSP-PLGA-ICG NPs.

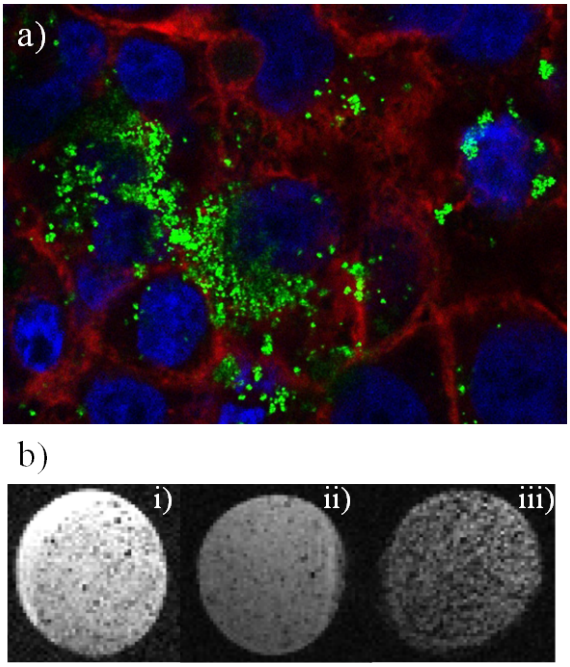

Figure S8: a) Confocal microscopy image of DXSP-PLGA-ICG NPs inside HeLa cells in the presence of an applied external magnetic field. Nuclei are blue-stained with DAPI, cystoplasm is stained with BODIPY-Phalloidin (in red), and DOXO fluorescence from the loaded NPs is colored in green. b) T_2-weighted MR images of i) untreated, and DXSP-PLGA-ICG NPs treated cells in the ii) absence and iii) presence of an external magnetic field. The image in the presence of the SPIONs-loaded hybrid NPs was darker than those obtained for untreated cells or cells treated with hybrid NPs in the absence of the applied magnetic field, further corroborating the efficacy of NP internalization by means of a magnetic-guided targeting strategy.

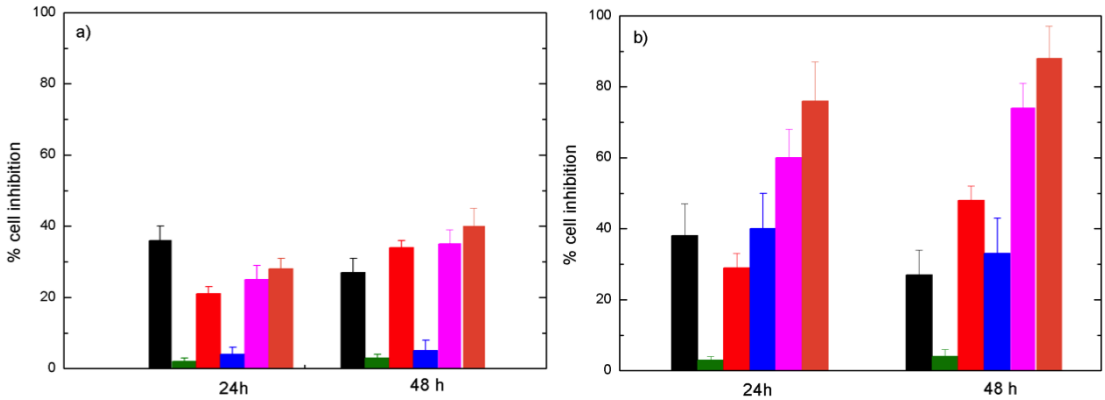

Figure S9. HeLa cell viabilities of free DOXO (black), SP-PLGA NPs (green), DXSP-PLGA NPs (red), SP-PLGA-ICG NPs (blue), DXSP-PLGA-ICG NPs (magenta) and DXSP-PLGA-ICG NPs in the presence of applied external magnetic field (orange) a) in the absence and b) presence of continuous NIR light (808 nm) of 2.5 W cm^{-2} for 5 min. Data shown as mean ± SD (n=3).

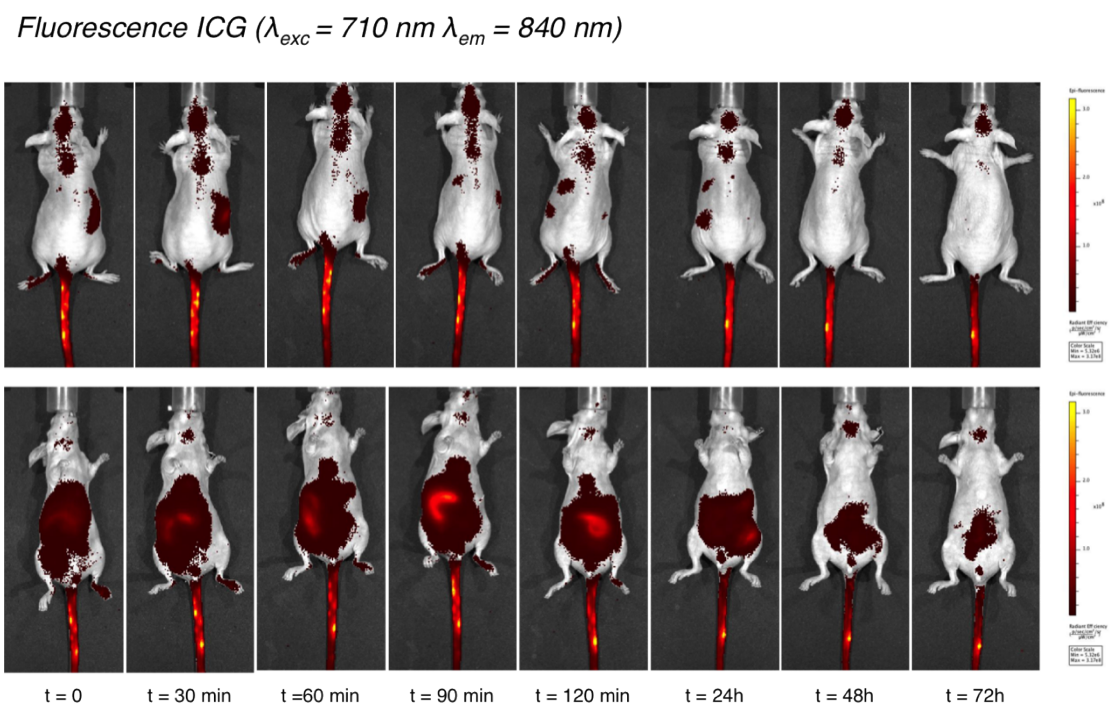

Figure S10: Time-lapse *in vivo* NIR images of MDA-MB-231 breast adenocarcinoma tumor-bearing mouse (top, dorsal position; bottom, ventral position) after intravenous tail injection of DXSP-PLGA-ICG NPs. The images denote the progressive decrease of fluorescence from RES organs.

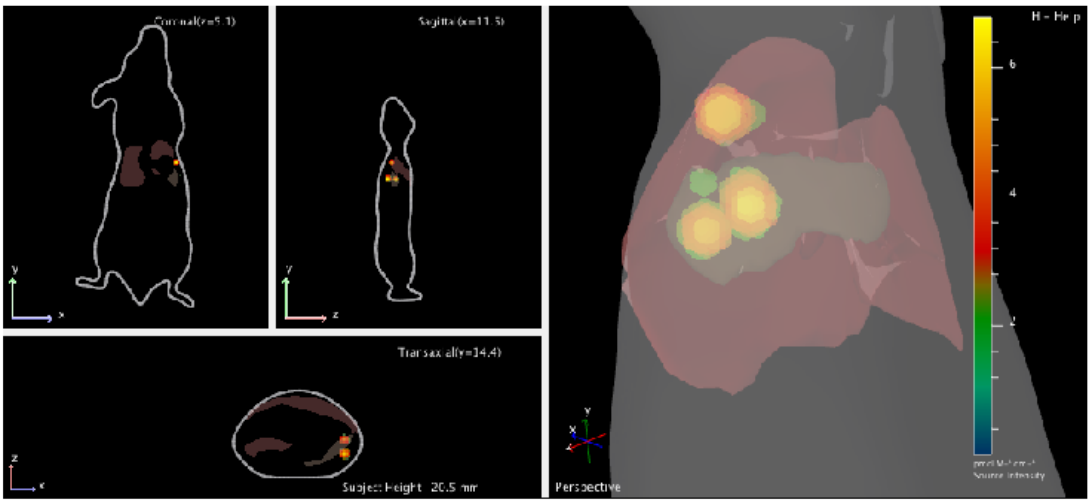

Figure S11: 3D-reconstructed fluorescence images of DXSP-PLGA-ICG NPs accumulation in the RES system after 6 h of incubation in a MDA-MB231 tumor-bearing mouse after intravenous tail injection of DXSP-PLGA-ICG NPs.

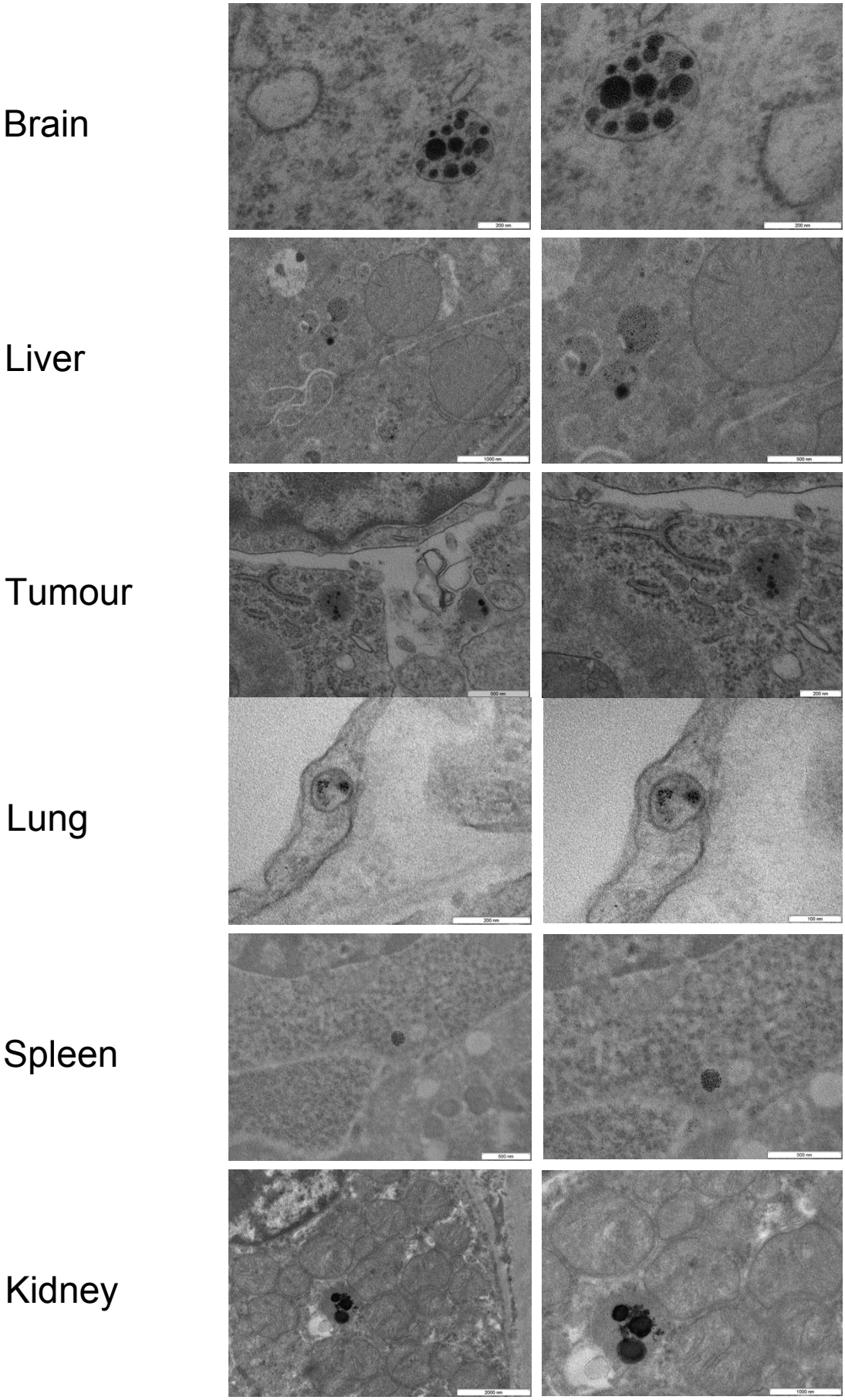

Figure S12: TEM images of sectioned tissues of different organs harvested 96 hours

upon treatment. The presence of some SP-PLGA-ICG NP can be observed. in several tissues, most notably brain, lung kidney and the tumour.

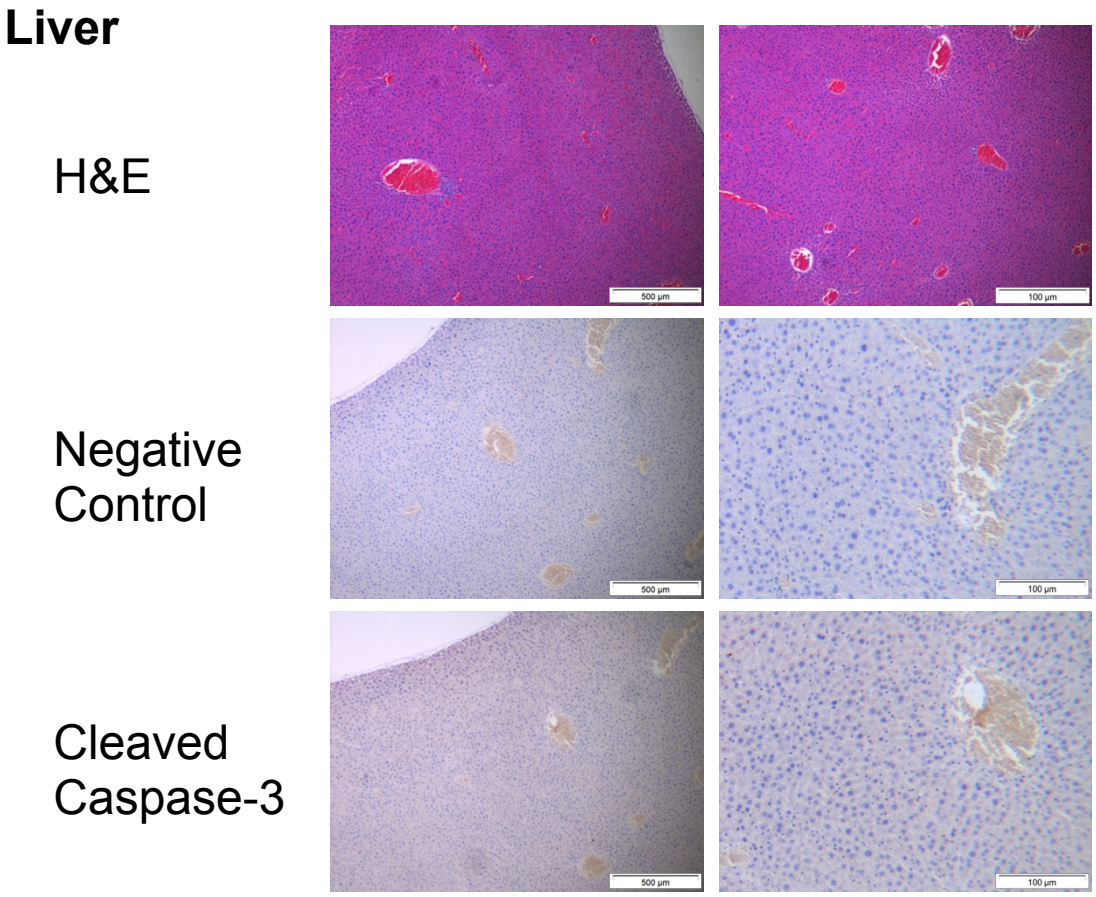

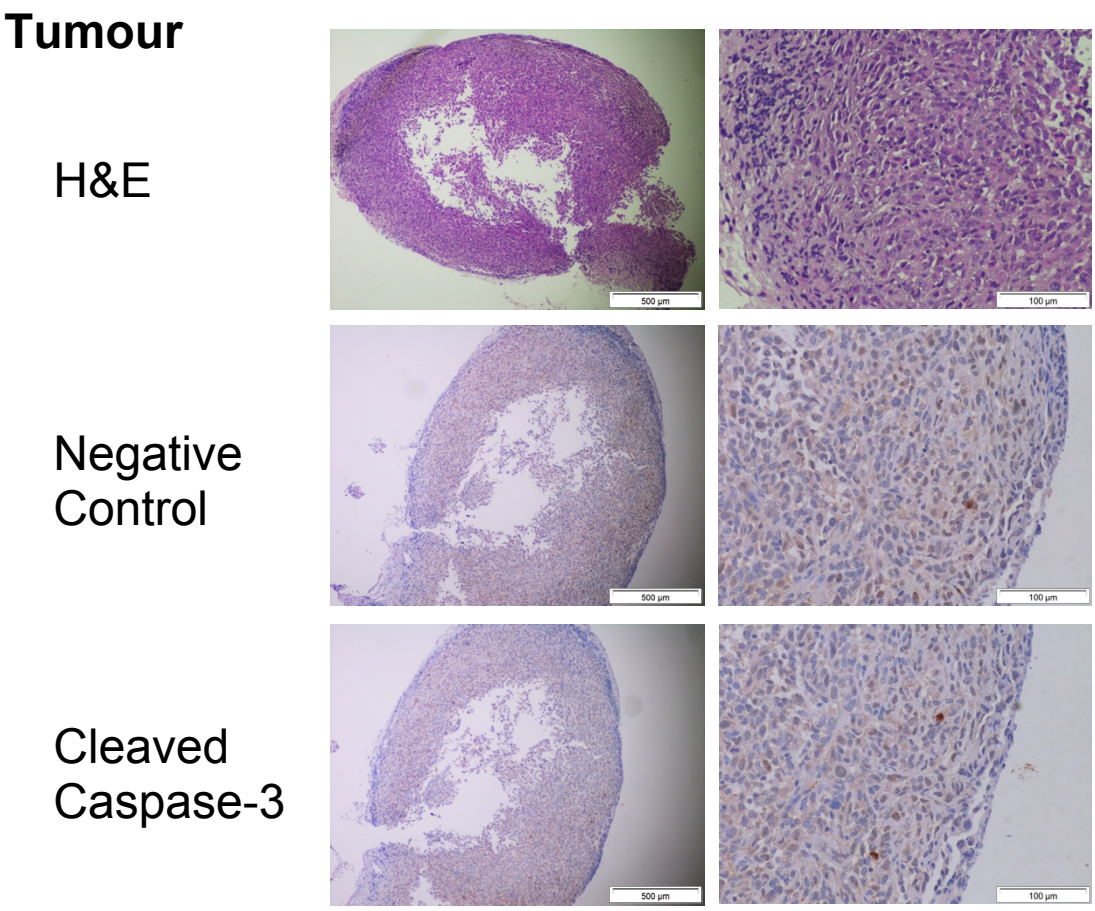

Figure S13: H&E staining and cleaved caspase-3 immunostaining of liver and tumor tissues. The lack of apoptotic cells in the liver indicates a very low or non-existent toxicity of SP-PLGA-ICG nanodevices.

References

1. L. H. Sperling, *Introduction to Physical Polymer Science*, John Wiley & Sons, New Jersey, 2006.
2. a) X. Song, Y. Zhao, S. Hou, F. Xu, R. Zhao, J. He, Z. Cai, Y. Li, Q. Chen, *Eur. J. Pharm. Biopharm.* 2008, **69**, 445; b) X. Song, Y. Zhao, W. Wu, Y. Bi, Z. Cai, Q. Chen, Y. Li, S. Hou, *Int. J. Pharm.* 2008, **35***0*, 320.
3. S. Benita, J. P. Benoit, F. Puisieux, C. Thies, *J. Pharm. Sci.* 1984, **73**, 1721.
4. a) J. Vandervoort, A. Ludwig, *Int. J. Pharm.* 2002, **238**, 77; b) U. Bilati, E. Allémann, E. Doelker, *Eur. J. Pharm. Sci.* 2005, **24**, 67.
5. S. Galindo-Rodriguez, E. Allémann, H. Fessi, E. Doelker, *Pharm. Res.* 2004, **21**, 1428.
6. a) S. K. Sahoo, J. Panyam, S. Prabha, V. Labhasetwar, *J. Control. Release* 2002, **82**, 105; b) S. Stolnik, S. Dunn, M. Garnett, M. Davies, A. A. Coombes, D. C. Taylor, M. P. Irving, S. C. Purkiss, T. F. Tadros, S. Davis, L. Illum, *Pharm. Res.* 1994, **11**, 1800.

7. Y. Ma, X. Liang, S. Tong, G. Bao, Q. Ren, Z. Dai, *Adv. Funct. Mater.* 2013, **23**, 815.
8. C. E. Astete, C. S. S. R. Kumar, C. M. Sabliov, *Colloids Surfaces A* 2007, **299**, 209.
9. J. Panyam, D. Williams, A. Dash, D. Leslie-Pelecky, V. Labhasetwar, *J. Pharm. Sci.* 2004, **93**, 1804.